# Observation of the particle-unstable nucleus $^{10}$N

A. Lépine-Szily,[1] J. M. Oliveira, Jr,[1,2,3] V. R. Vanin,[1] A. N. Ostrowski,[4] R. Lichtenthäler,[1] A. Di Pietro,[4] V. Guimarães,[1] A. M. Laird,[4] L. Maunoury,[5] G. F. Lima,[1,3] F. de Oliveira Santos,[5] P. Roussel-Chomaz,[5] H. Savajols,[5] W. Trinder,[5] A. C. C. Villari,[5] and A. de Vismes[5]

[1]*Instituto de Fisica, Universidade de São Paulo, Caixa Postal 66318, 05315-970 São Paulo, Brazil*
[2]*CETEC, Centro de Ciências Exatas, Universidade de Sorocaba, Sorocaba, Brazil*
[3]*FACENS, Faculdade de Engenharia de Sorocaba, Sorocaba, Brazil*
[4]*Department of Physics & Astronomy, University of Edinburgh, Edinburgh EH9 3JZ, United Kingdom*
[5]*GANIL, Boulevard Henri Becquerel, Boîte Postale 5027, F-14021 Caen Cedex, France*

(Received 21 December 2001; published 9 May 2002)

For the first time evidence of the ground state of the proton-rich, unbound nucleus $^{10}$N has been found in the multinucleon transfer reaction $^{10}$B($^{14}$N,$^{14}$B)$^{10}$N. The observed resonance of $^{10}$N has a mass excess of 38.8(4) MeV and a width of $\Gamma = 2.3(16)$ MeV, close to the Audi-Wapstra estimation of 38.5(4) MeV. $^{10}$N is the last missing $A = 10$ multiplet partner.

DOI: 10.1103/PhysRevC.65.054318 PACS number(s): 21.10.Dr, 25.70.Hi, 27.20.+n

## I. INTRODUCTION

Light nuclei with large neutron (or proton) excess have raised much interest in recent years, both from experimental and theoretical points of view. They provide a benchmark for nuclear structure models under extreme conditions of high isospin and low binding energies. Among their interesting aspects, we can cite the inversion of the normal shell model ordering for energy levels, for example, the lowering of the $2s_{1/2}$ level below the $1p_{1/2}$ in $^{11}$Be. The ground state of the neutron-rich $^{11}$Be nucleus is $1/2^+$, instead of the predicted $1/2^-$. The same inversion can be observed in its mirror partner, the unbound neutron deficient $^{11}$N nucleus recently studied by transfer reactions [1,2]. The excited resonances of $^{11}$N show a level scheme similar to its mirror partner $^{11}$Be, predicted by the charge independence of the nuclear force. The quenching of the shell model magic numbers, e.g., $N = 8$ near to the neutron drip line is another unusual aspect recently observed. Among the unexpected properties observed for nuclei on the neutron drip line, the most spectacular is the existence of a neutron halo, present in some neutron-rich light nuclei such as $^{11}$Li, $^{11}$Be, $^{8}$He, $^{6}$He, etc. The largest effect can be seen in $^{11}$Li, where two weakly bound valence neutrons penetrate the potential barrier, extending well beyond the radius of the core nucleus. The study of the unbound $^{10}$Li is important for the understanding of the structure of $^{11}$Li. This nucleus has been extensively studied in the past years, without reaching a consensus on its structure [3–12]. The unbound $^{10}$N nucleus, its mirror partner, should have a similar structure and level scheme. It is predicted to be unbound: recent extrapolation [13] predicts its ground state to be $\sim 2.3(4)$ MeV above the proton decay threshold of $^{9}C + p$. The study of unbound, proton-rich, light nuclei, such as $^{10,11}$N, can shed some light on these interesting problems. The structure of these unbound nuclei can also be relevant in astrophysical calculations.

Recent measurements of the three particle transfer reactions $^{12}$C($^{14}$N,$^{15}$C)$^{11}$N [1] and $^{10}$B($^{14}$N,$^{13}$B)$^{11}$N [2] have shown that the latter reaction was better adapted to populate the ground state and excited resonances of the recoiling $^{11}$N nucleus. Although the $Q$ value of the reaction is more negative and the cross sections are somewhat lower, nevertheless the reaction is less selective, populating all resonances with similar strength.

There are no three-nucleon transfer reactions with stable target and beam combinations (stable beams are much more intense than radioactive beams), which yield $^{10}$N as a recoil nucleus. Thus, we have chosen the four-nucleon transfer reaction $^{10}$B($^{14}$N,$^{14}$B)$^{10}$N to populate the resonances of the recoiling unbound $^{10}$N nucleus. The $Q$ value for this reaction, despite being very negative, is comparable to the $Q$ values of the other possible four-nucleon transfer reactions, based on $^{12}$C or $^{14}$N targets. The same combination of beam and target has given good results for the study of $^{11}$N. As a matter of fact, these measurements were performed simultaneously for the $^{10,11}$N nuclei.

## II. EXPERIMENTAL METHOD

We have studied at the Grand Accelerateur National d'Ions Lourds (GANIL) the unbound $^{10}$N nucleus using the multinucleon transfer reaction $^{10}$B($^{14}$N,$^{14}$B)$^{10}$N. We have chosen the energy of the $^{14}$N beam to be 30$A$ MeV, where the highest yield of transfer cross section is expected. The transfer probability, in general, exhibits a maximum at the Fermi velocitiy of the valence nucleons [14], which would correspond to 20–30 $A$ MeV for the incident beam energy. The isotopically enriched $^{10}$B target was a ''sandwich'' of four targets with thickness of 0.1 mg/cm$^2$ each. The $^{10}$B targets had some content of $^{11}$B and impurities of $^{16}$O and $^{12}$C. To determine the contribution of these other isotopes to the spectrum, we also performed measurements on an isotopically enriched $^{11}$B target (0.2 mg/cm$^2$), on a ''sandwich'' of two $Li_2O$ targets (each of them 0.15 mg/cm$^2$ evaporated on 50 $\mu$g/cm$^2$ carbon backing), and on a 0.5-mg/cm$^2$ carbon target.

The ejectiles were analyzed by the high-precision magnetic spectrometer SPEG [15]. The laboratory angles subtended by SPEG were $\theta = 1.2° - 4.5°$ and $\phi = 0° \pm 2.0°$ in the

 

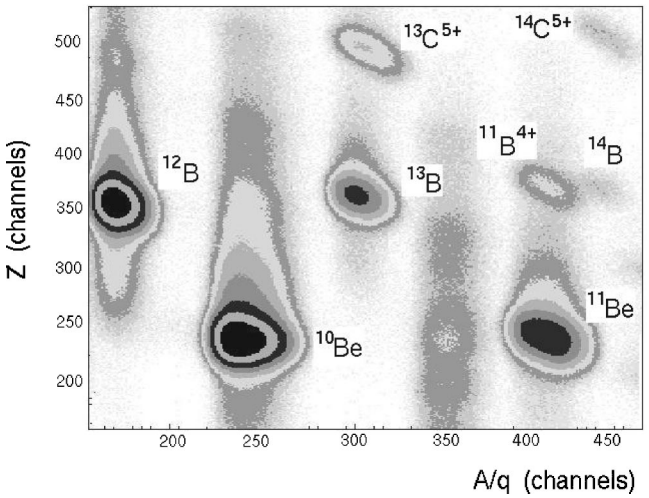


FIG. 1. Part of the two-dimensional particle identification spectrum measured on the $^{10}$B target. Due to the very good resolution all mass groups are well separated, in particular, the clear separation between the $^{14}$B and the $^{11}Be^{4+}$ nuclides is to be observed.

horizontal and vertical planes, respectively. The standard SPEG detection system was used [15]; it includes two drift chambers, an ionization chamber, and a plastic scintillator for the focal-plane position, the energy-loss ($\Delta E$), and residual energy measurements, respectively. The time of flight (TOF) was measured using a fast scintillator signal with respect to the cyclotron radio frequency. The two-dimensional particle identification spectrum ($Z$ vs $A/q$, where $Z$ and $A/q$ are calculated from $\Delta E$ and TOF) allows a clear separation of all mass groups. We present in Fig. 1 a typical particle identification spectrum measured with the $^{10}$B target. Three $Z$ values can be observed on the expanded spectrum corresponding to Be, B, and C isotopes, where the C isotopes were observed in the $q=5^+$ charge state. We can observe the very good resolution of the SPEG detection system in $Z$ and $A/q$. In particular, the $^{14}$B ejectiles were produced with a very low cross section ($2p-2n$ exchange), however they could be identified and well separated from the much more intense $^{11}B^{4+}$ mass group. The reaction products were momentum analyzed by the horizontal and vertical position measurements carried out by the two drift chambers. The positions $(x,y)$ and the angles $(\theta,\phi)$ of each particle in the focal plane were reconstructed by two position measurements 1.2 m apart. The scattering angles $\Theta_{lab}$, calculated from the measured $(\theta,\phi)$ angles, range from 1.2° to 4.9° and the medium angle was 3.05°. Two-dimensional plots of the focal-plane position versus scattering angle were used to perform the kinematical corrections.

### III. RESULTS

The momentum and energy calibrations were easily performed with the ($^{14}$N,$^{12}$B) reaction on the $^{10}$B, $^{11}$B, $Li_2O$, and $^{12}$C targets. The $Q$ values and ejectile laboratory energies $E_{lab}$ leading to the ground states of the ($^{14}$N,$^{12}$B) reactions on the target components are

$$^{10}\mathrm{B}(^{14}\mathrm{N},^{12}\mathrm{B})^{12}\mathrm{N}, \quad Q_0=-15.793 \text{ MeV},$$
$$E_{lab}(\text{g.s.})=403.1 \text{ MeV}, \tag{1}$$
$$^{11}\mathrm{B}(^{14}\mathrm{N},^{12}\mathrm{B})^{13}\mathrm{N}, \quad Q_0=-7.184 \text{ MeV},$$
$$E_{lab}(\text{g.s.})=413.1 \text{ MeV}, \tag{2}$$
$$^{16}\mathrm{O}(^{14}\mathrm{N},^{12}\mathrm{B})^{18}\mathrm{Ne}, \quad Q_0=-20.562 \text{ MeV},$$
$$E_{lab}(\text{g.s.})=400.1 \text{ MeV}, \tag{3}$$
$$^{7}\mathrm{Li}(^{14}\mathrm{N},^{12}\mathrm{B})^{9}\mathrm{B}, \quad Q_0=-8.013 \text{ MeV},$$
$$E_{lab}(\text{g.s.})=409.8 \text{ MeV}, \tag{4}$$
$$^{12}\mathrm{C}(^{14}\mathrm{N},^{12}\mathrm{B})^{14}\mathrm{O}, \quad Q_0=-18.513 \text{ MeV},$$
$$E_{lab}(\text{g.s.})=401.0 \text{ MeV}. \tag{5}$$

In Fig. 2 are shown the energy spectra of the intense ($^{14}$N,$^{12}$B) reactions on the $^{10}$B, $^{11}$B, $^{16}$O, and $^{12}$C targets, with an energy binning of 166 keV/channel. The first panel [Fig. 2(a)] shows the energy spectrum of the $^{12}$B ejectiles measured on the $^{10}$B target.

The most energetic peaks (between 404 and 413 MeV) are due to reactions on the $^{11}$B impurity content of the $^{10}$B target and can be compared to the peaks in the lower figure [Fig. 2(b)], measured on the isotopically enriched $^{11}$B target. The correspondence between the two spectra allows to calculate the amount of impurity content in the $^{10}$B target and subtract its contribution. The peaks observed in the energy spectra of the $^{11}$B($^{14}$N,$^{12}$B)$^{13}$N reactions correspond to well known levels of the $^{13}$N nucleus at 0.00 MeV ($1/2^-$), 3.55 MeV ($5/2^+$), 7.15 MeV ($7/2^+$), 8.91 MeV ($1/2^-$), and 11.53 MeV ($5/2^+$). Only the ground state of the $^{13}$N nucleus is bound, all excited states are unbound. The $1/2^+$ resonance at 2.36 MeV is practically unpopulated in this reaction. Each level populated in the reaction appears as a doublet in the energy spectrum: the more energetic peak corresponds to the $^{12}$B ejectile in its $1^+$ ground state and the lower energy peak (indicated by *) corresponds to the $^{12}$B ejectile in its $2^+$ excited state at 0.953 MeV. Other bound excited states of $^{12}$B at 1.673 MeV ($2^-$), 2.621 MeV ($1^-$), and 2.723 MeV ($0^+$) are not populated in this reaction. The differential cross section at $\Theta_{lab}=3.05°$ for the $^{11}$B($^{14}$N,$^{12}$B$_{\text{g.s.}}$)$^{13}$N$_{\text{g.s.}}$ reaction is 15(2) $\mu$b/sr.

The peaks corresponding to the $^{10}$B($^{14}$N,$^{12}$B)$^{12}$N reaction begin at $E_{lab}=403$ MeV in the upper energy spectrum, measured on the $^{10}$B target. The peaks correspond to well known levels of the $^{12}$N nucleus at 0.00, 0.96+1.19,1.8, 3.13 and 4.14 MeV. The peak around $E^*=1$ MeV is broader and can be due to the population of the 0.96+1.19 MeV doublet in $^{12}$N with the $^{12}$B ejectile in its ground state or the 0.953 MeV excited state of the $^{12}$B with the $^{12}$N in ground state. The small peak at 401 MeV can be due to the 1.8 MeV resonance in $^{12}$N or the mutual excitation of the $^{12}$B ejectile(0.953 MeV) and the unbound $^{12}$N resonances at 0.96

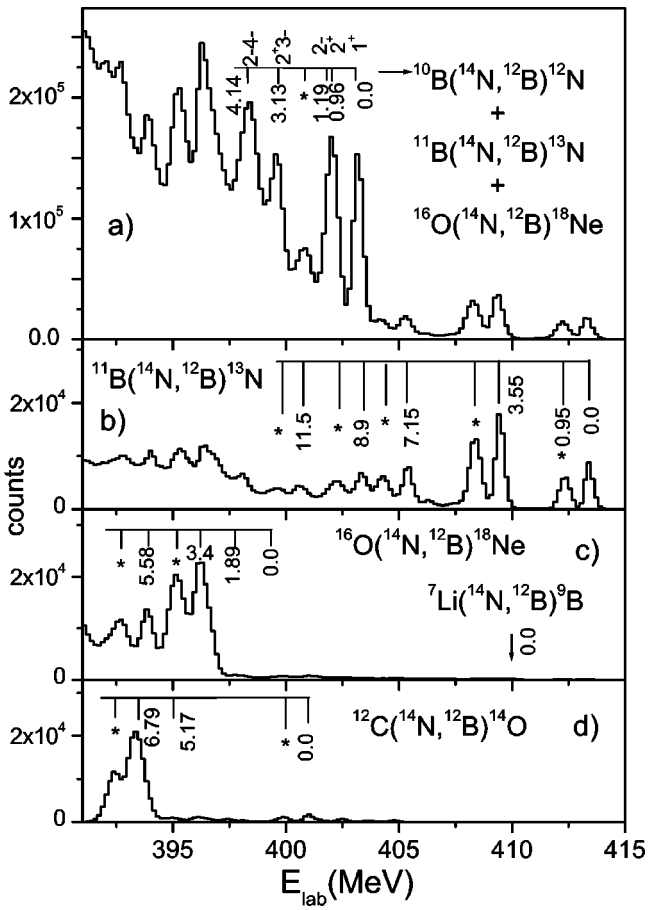


FIG. 2. Energy spectra (166 keV/channel) of the ($^{14}$N,$^{12}$B) reactions on the $^{10}$B (a), $^{11}$B (b), $Li_2O$ (c), and $^{12}$C (d) targets used in the experiment. The peaks correspond to well known levels of the final nuclei $^{12}$N, $^{13}$N, $^{18}$Ne, and $^{14}$O, with the ejectile $^{12}$B in its ground state or in its first excited state at $E^*=0.953$ MeV, indicated by an asterisk. The figure also shows that the $^{10}$B target had $^{11}$B and $^{16}$O contamination and the comparison between spectra has allowed the determination of the amount of impurity content in the $^{10}$B target, as well as the precise energy calibration of the energy spectra. The subtraction of impurities can thus be performed. Details of the analysis are described in the text.

$+1.19$ MeV. The differential cross section at $\Theta_{lab}=3.05°$ for the $^{10}$B($^{14}$N,$^{12}$B$_{g.s.}$)$^{12}$N$_{g.s.}$ reaction is 6.4(9) $\mu$b/sr.

The energy spectrum of the $^{12}$B ejectiles measured on the $Li_2O$ target is presented in Fig. 2(c) and shows that this target was well positioned and endured the beam. The yield due to the $^{7}$Li($^{14}$N,$^{12}$B)$^{9}$B reaction is negligibly small when compared to the $^{16}$O($^{14}$N,$^{12}$B)$^{18}$Ne reaction. The ground and first excited states of the $^{18}$Ne nucleus are weakly populated while the $4^+$ state at 3.37 MeV and a state at 5.58 MeV are strongly excited. These same states can be observed on the energy spectrum of the $^{10}$B target, allowing to obtain its amount of oxygen impurity content from the comparison of both spectra. The differential cross section at $\Theta_{lab}=3.05°$ for the $^{16}$O($^{14}$N,$^{12}$B$_{g.s.}$)$^{18}$Ne(3.4 MeV) reaction is 240(34) $\mu$b/sr and for the $^{7}$Li($^{14}$N,$^{12}$B$_{g.s.}$)$^{9}$B$_{g.s.}$ reaction is 5(1) $\mu$b/sr.

In Fig. 2(d) the energy spectrum measured on the $^{12}$C target is presented. The ground state of the $^{14}$O nucleus can be seen as a small peak at 401 MeV, as well as the first excited unbound resonance at 5.17 MeV, while a resonance at 6.79 MeV is strongly populated. The estimation of the amount of $^{12}$C impurity in the $^{10}$B target is subject to a larger error due to its position at larger excitation energies, but due to this same reason its importance will be negligible at the energies of interest. The differential cross section at $\Theta_{lab}=3.05°$ for the $^{12}$C($^{14}$N,$^{12}$B$_{g.s.}$)$^{14}$O(6.79 MeV) reaction is 150(20) $\mu$b/sr.

The ($^{14}$N,$^{13}$B) reactions on the $^{10}$B, $^{11}$B, $^{16}$O, and $^{12}$C targets were also measured simultaneously. The results have already been published [2] and confirm the same energy calibrations and target contaminations obtained by the ($^{14}$N,$^{12}$B) reactions. The analysis of the $^{10}$B($^{14}$N,$^{13}$B)$^{11}$N reaction allowed the observation of the ground state and six excited states of $^{11}$N [2].

### A. The ($^{14}$N,$^{14}$B) reactions

The $Q$ values and ejectile laboratory energies $E_{lab}$ leading to ground states of the ($^{14}$N,$^{14}$B) reactions on the target components are

$$^{10}\mathrm{B}(^{14}\mathrm{N},^{14}\mathrm{B})^{10}\mathrm{N}, \quad Q_0=-47.250 \ \mathrm{MeV}, \quad E_{lab}(\mathrm{g.s.})=373.2 \ \mathrm{MeV}, \tag{6}$$

$$^{11}\mathrm{B}(^{14}\mathrm{N},^{14}\mathrm{B})^{11}\mathrm{N}, \quad Q_0=-36.750 \ \mathrm{MeV}, \quad E_{lab}(\mathrm{g.s.})=385.4 \ \mathrm{MeV}, \tag{7}$$

$$^{16}\mathrm{O}(^{14}\mathrm{N},^{14}\mathrm{B})^{16}\mathrm{Ne}, \quad Q_0=-49.527 \ \mathrm{MeV}, \quad E_{lab}(\mathrm{g.s.})=372.9 \ \mathrm{MeV}, \tag{8}$$

$$^{7}\mathrm{Li}(^{14}\mathrm{N},^{14}\mathrm{B})^{7}\mathrm{B}, \quad Q_0=-33.764 \ \mathrm{MeV}, \quad E_{lab}(\mathrm{g.s.})=387.1 \ \mathrm{MeV}, \tag{9}$$

$$^{12}\mathrm{C}(^{14}\mathrm{N},^{14}\mathrm{B})^{12}\mathrm{O}, \quad Q_0=-52.680 \ \mathrm{MeV}, \quad E_{lab}(\mathrm{g.s.})=368.3 \ \mathrm{MeV}, \tag{10}$$

where we have used our recently measured [2] mass excess value of 24.618(50) MeV for the $^{11}$N ground-state resonance, $\Delta=38.5(4)$ MeV for the $^{10}$N [13], and the Audi-Wapstra [16] mass excess values for the other nuclei.

The ejectile $^{14}$B has only two particle-stable states, its ground state with $J^\pi=2^-$ and its first excited state at 0.74 MeV excitation energy with $J^\pi=1^-$. The $Q$ values in the Eqs. (6)–(10) were calculated with $^{14}$B in its ground state. The $^{10}$N ground state (probably also a $2^-$ state, by analogy with $^{10}$Li) is probably more strongly populated in conjunction with the $2^-$ ground state of the $^{14}$B ejectile, than with its $1^-$ first excited state. The reason for this selectivity is that in this case all nuclei involved in the reaction have an unnatural parity ($^{10}$B and $^{14}$N have, respectively, $3^+$ and $1^+$ ground states).

In Fig. 3 are shown the energy spectra of the weak ($^{14}$N,$^{14}$B) reactions on the $^{10}$B, $^{11}$B, $^{16}$O, and $^{12}$C targets,

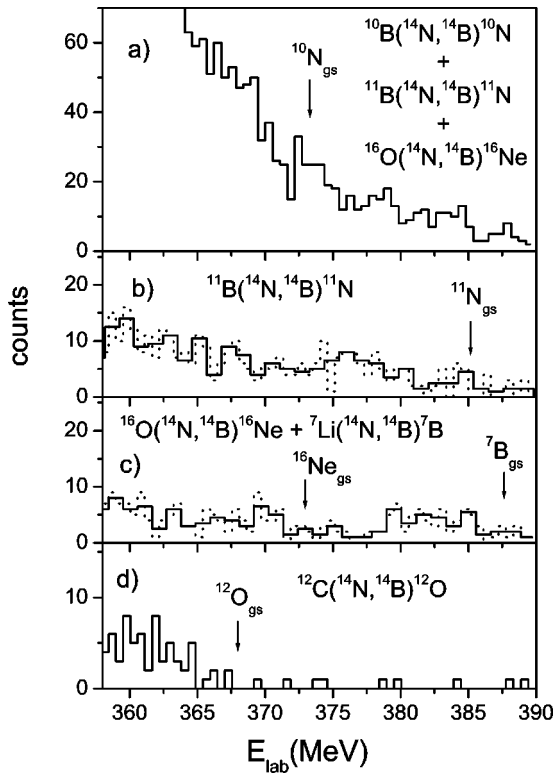


FIG. 3. Energy spectra (550 keV/channel) of the ($^{14}$N,$^{14}$B) reactions on the $^{10}$B (a), $^{11}$B (b), $Li_2O$ (c), and $^{12}$C (d) targets. The dotted lines in (b) and (c) are the spectra with energy binning of 550 keV/channel. The solid lines were obtained by an additional compression of a factor 2 on the energy scale. The arrows indicate the positions of the ground-state energies of the various reactions.

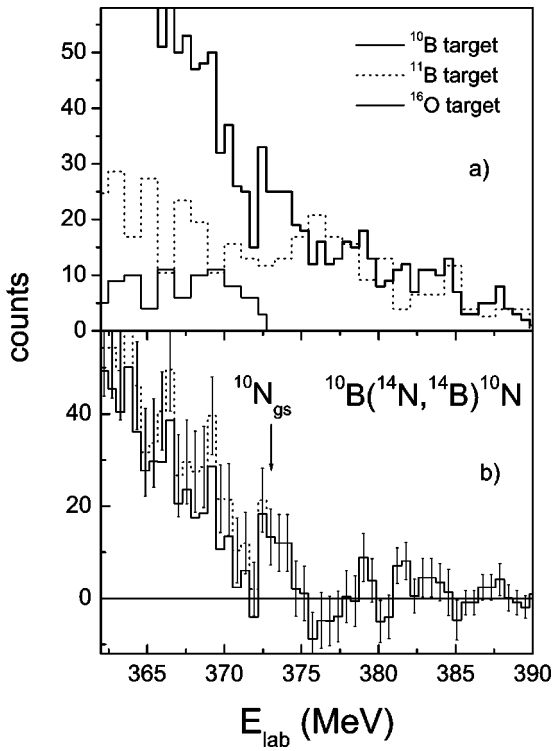


FIG. 4. (a) Energy spectra (550 keV/channel) of the ($^{14}$N,$^{14}$B) reactions on the $^{10}$B target (solid line), on the $^{11}$B target (dotted line), and on the $Li_2O$ target (solid line), where counts with $E_{lab} \geqslant 372.88$ MeV were rejected. The normalizations factors were determined from ($^{14}$N,$^{12}$B) reactions and took into account the amount of impurity content in the $^{10}$B target. (b) Energy spectrum obtained after subtraction of the target contaminants. The two curves correspond to two different normalization factors for the $^{16}$O subtraction. The statistical error of the subtracted spectrum is also indicated.

with an energy binning of 550 keV/channel. All energy spectra present very low statistics, due to the very negative $Q$ values. The energy spectra of the ($^{14}$N,$^{12}$B) (Fig. 2) and ($^{14}$N,$^{14}$B) (Fig. 3) reactions were obtained simultaneously (see Fig. 1) using the same targets, thus the same momentum and energy calibration can be used for both reactions and the amount of impurity contents determined with the ($^{14}$N,$^{12}$B) reactions can be used for the subtraction of the energy spectra of the ($^{14}$N,$^{14}$B) reactions.

The upper panel [Fig. 3(a)], which has the best statistics, shows the energy spectrum of the $^{14}$B ejectiles measured on the $^{10}$B target. It clearly shows a broad peak around $E_{lab} = 373$ MeV ejectile energy, which corresponds to the expected position of the ground-state resonance of $^{10}$N [13]. This peak is superimposed on a background, which is fairly flat and low between 375 and 390 MeV and which increases rapidly for lower ejectile energies. The differential cross section corresponding to the ground-state resonance of $^{10}$N is $0.7 \pm 0.2$ nb/sr.

The energy spectrum measured on the $^{11}$B target [Fig. 3(b)] presents no statistically significant peaks and its energy axis was further compressed by a factor of 2 in order to diminish statistical fluctuations. The solid line corresponds to the compressed spectrum, while the dotted line to the spectrum before additional compression. When we compare the spectra on $^{10}$B and $^{11}$B targets [Figs. 3(a) and 3(b)], we verify that the slowly decreasing background between 375 and 390 MeV, in Fig. 3(a), is due to reactions on the $^{11}$B content of the $^{10}$B target. Using the normalization factor (of the $^{11}$B impurity amount in the $^{10}$B target) obtained from the ($^{14}$N,$^{12}$B) reaction and subtracting the normalized spectrum of Fig. 3(b) from that of Fig. 3(a), the whole flat background between between 375 and 390 MeV disappears. This is shown in Fig. 4. Thus the subtraction of the $^{11}$B impurity content can be performed in a straightforward way. The differential cross section corresponding to the $^{11}B(^{14}N,^{14}B)^{11}N$ reaction is 4(1) nb/(sr MeV) between 372.5–373.5 MeV.

In Fig. 3(c), we present the $^{14}$B spectrum on the $Li_2O$ target. The solid line corresponds to the compressed spectrum while the dotted line corresponds to the spectrum before additional compression, as in Fig. 3(b). Again the $^{7}Li(^{14}N,^{14}B)^{7}B$ reaction has a smaller $Q$ value and the position of the $^{7}B_{g.s.}$ resonance at 387.1 MeV is indicated by an arrow. The threshold for the $^{16}O(^{14}N,^{14}B)^{16}Ne$ reaction is at 372.88 MeV. Thus, the yield with $E_{lab} \geqslant 372.88$ MeV can come only from the $^{7}$Li content of the target and was rejected. Unfortunately this yield is not negligible, indicating that not only at $E_{lab} \geqslant 372.88$ MeV but the whole energy spectrum is affected by the $^{7}Li(^{14}N,^{14}B)^{7}B$ reaction.

Thus the $^{14}$B spectrum measured on the $Li_2O$ target and multiplied by the normalization factor determined from the $^{16}O(^{14}N,^{12}B)^{18}Ne$ reaction measured with the same $Li_2O$ target is overestimated for $E_{lab} \leqslant 372.88$ MeV. The spectrum used for subtraction has no counts with $E_{lab} \geqslant 372.88$ MeV and different normalization factors were tried as will be explained below. The differential cross section corresponding to the $^{7}Li(^{14}N,^{14}B)^{7}B + ^{16}O(^{14}N,^{14}B)^{16}Ne$ reactions between 372.5 and 373.5 MeV is 3(2) nb/(sr MeV).

In Fig. 3(d), we present the $^{14}$B spectrum on the $^{12}$C target. The ground state of the $^{12}C(^{14}N,^{14}B)^{12}O$ reaction is located at $E_{lab} = 368$ MeV and its influence in the region of interest is negligible. Its contribution will not be subtracted. The differential cross section corresponding to the $^{12}C(^{14}N,^{14}B)^{12}O$ reaction between 363.5 and 364.5 MeV is 8(3) nb/(sr MeV).

In Fig. 4(a) (upper panel) we show the energy spectra (550 keV/channel) of the $(^{14}N,^{14}B)$ reactions on the $^{10}$B target (solid line), on the $^{11}$B target (dotted line), and on the $Li_2O$ target (solid line) with the normalizations taking into account the amount of impurity content in the $^{10}$B target. In Fig. 4(b) we show the energy spectrum of the $^{10}B(^{14}N,^{14}B)^{10}N$ reaction obtained after the subtraction of the normalized experimental spectra of the $^{11}B(^{14}N,^{14}B)^{11}N$ and $^{16}O(^{14}N,^{14}B)^{16}Ne$ reactions, as explained above. The energy binning of the spectrum is 550 keV per channel. Two curves are shown, they correspond to two different normalization factors for the subtraction of the $^{16}$O content in the target. In order to have the subtracted spectrum always positive on the average, the normalization factor should not be further increased. The statistical error of the subtracted spectrum is also shown in Fig. 4(b).

In Fig. 4(b) (lower panel) a broad peak is observed around 373 MeV ejectile energy, which corresponds to the expected position of the ground-state resonance of $^{10}$N [13]. The fast rising background in the subtracted spectrum is the result of the three- and four-body fragmentation reactions $^{10}B + ^{14}N \rightarrow ^{14}B + ^{9}C + p$ and $^{10}B + ^{14}N \rightarrow ^{14}B + ^{8}B + p + p$ and can be calculated by phase space considerations [17]. The form, slope, and threshold of the background spectra are determined by the $Q$ and mass values and number of fragments, the normalization factors being free parameters. The reaction $Q$ values of the $^{9}C_{g.s.} + p$ and $^{8}B_{g.s.} + p + p$ thresholds are, respectively, $Q = -44.952$ and $-46.249$ MeV. The recoiling nuclei can be excited and the $Q$ values can be more negative.

The $Q$ value of the $^{10}B(^{14}N,^{14}B)^{10}N$ reaction can be determined from the position of the peak in the $^{14}$B energy spectrum, the masses, and relativistic kinematics. The mass excess of $^{10}$N is calculated from the $Q$ value and from the masses, through the equation $\Delta(^{10}N) = \Delta(^{14}N) + \Delta(^{10}B) - \Delta(^{14}B) - Q$, where $\Delta$ are the mass excess values. The decay energy above the proton decay threshold can be calculated by $E_{decay} = \Delta(^{10}N) - \Delta(^{9}C_{g.s.}) - \Delta(p)$.

In the following we will analyze the subtracted spectrum [Fig. 4(b), solid line] and find statistical criteria to show that the existence of a resonance has a high probability. In Fig. 5 we present the same subtracted spectrum as a function of the decay energy, the results of two sets of fits are presented: in (lower part) the calculation assumes the existence of a peak, due to the population of the $^{10}N_{g.s.}$ together with a fitted background due to the three- and four-body fragmentations. In (upper part) only the presence of three- and four-body fragmentation is assumed, without any resonance in the spectrum.

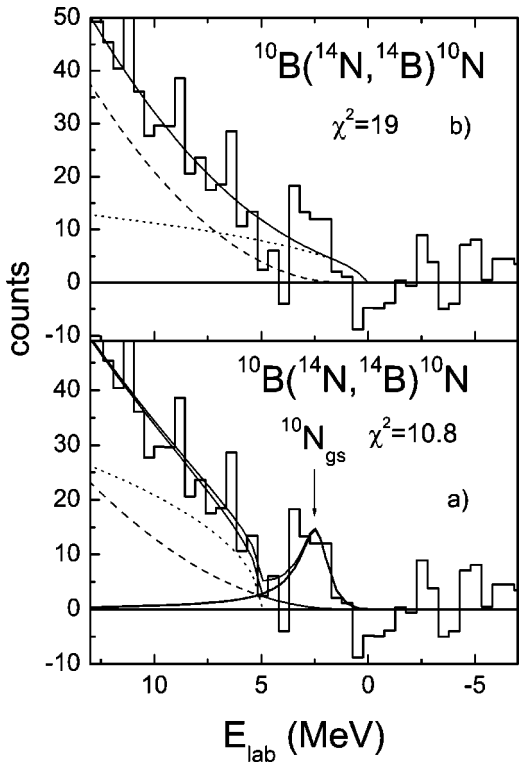


FIG. 5. (a) (lower panel) Energy spectrum (550 keV/channel) of the $^{10}B(^{14}N,^{14}B)^{10}N$ reaction, obtained after subtraction of target contaminants. Solid line represents best fit with a Breit-Wigner resonance (solid line) summed with three- (dotted line) and four-body (dashed line) fragmentation background. The three-body background is taking into account the excitation of decay products. The quality of the fit is indicated by $\chi^2$ values over ten degrees of freedom. (b) (upper panel) The same energy spectrum fitted by the sum (solid line) of three- (dot) and four-body (dashed) fragmentation background, without any resonance.

The peak was fitted with a Breit-Wigner line shape,

$$\frac{d\sigma}{dE} = \frac{A\Gamma_l(E)}{[E_r + \Delta_l(E) - E]^2 + 1/4[\Gamma_l(E)]^2}, \qquad (11)$$

where $A$ is the strength, fitted to the height of the peak, and $E_r$ is the resonance energy. The decay width $\Gamma_l(E)$ and the shift $\Delta_l(E)$ are given in terms of the reduced width $\gamma_l^2$, which contains the spectroscopic information on the specific nuclear state, the penetration factor $P_l(E)$, and the shift function $S_l(E)$, $\Gamma_l(E) = 2P_l(E)\gamma_l^2$ and $\Delta_l(E) = -[S_l(E) - S_l(E_r)]\gamma_l^2$. $P_l(E)$ is the penetration factor, which describes the probability of an $l$ state proton penetrating into

the Coulomb + centrifugal barrier, when the resonant state of $^{10}$N situated at energy $E=E_{decay}$ above the threshold decays into a proton + $^{9}$C. $P_l(E)$ and $S_l(E)$ are defined in terms of regular and irregular Coulomb wave functions and were calculated at the matching radius $a=4.46$ fm. The free parameters were A, $\gamma_l^2$, and $E_r$.

The calculated background shown in Fig. 5(a) was the sum of two different components as follows.

(i) The contribution of the three-body fragmentation cross section calculated by phase space calculations [dotted line in Fig. 5(a)]. The normalization and the energy threshold were the free parameters of the fit. The variation of the energy threshold corresponds to the excitation of the decay products. The best fit yielded a total excitation energy of 5.1(2) MeV for the decay products. The $^{9}$C has no particle-stable excited states. Its proton separation energy is $S_p=1.296$ MeV and one excited resonance is known at 2.218 MeV excitation energy. Thus the energy threshold with 5.12 MeV excitation energy can come from an excited resonance at this energy in $^{9}$C, or at 4.4 MeV together with the excitation of the $^{14}$B ejectile. If the resonances have enough half-life, the kinematics is defined before the decay and the form of the continuous energy spectrum is not modified. If it is modified, the four-body fragmentation decay will take this into account.

(ii) The four-body fragmentation cross section calculated by phase space calculations [dashed line in Fig. 5(a)]. The sum of both contributions accounts very well for the fast rising background for $E_{decay}\geqslant 5$ MeV. The total $\chi^2$ value of the best fit between $E_{decay}=0$ and 7.8 MeV is 10.8 for ten degrees of freedom.

In the calculation shown in Fig. 5(a), we assumed the existence of one $l=0$ resonance superimposed on the previously described background and determined its position, width, and amplitude (as well as the parameters of the background) by a least squares fit to the data in the peak region between $E_{decay}=0$ and 12 MeV. The calculation presented in Fig. 5(a) corresponds to the best fit to the data. The fitted value of the resonance decay energy is $E_r=2.64(40)$ MeV and the fitted width of the resonance is $\Gamma_l(E_r)=2.3(16)$ MeV, corresponding to a reduced width of $\gamma_0^2=1.2(8)$ MeV. The area of the peak is $67\pm 17$ counts, thus it has a statistical significance of $4.0\sigma$, which means probability of occurrence of 99%. Adding a resonance shifted by 0.74 MeV, with the same width, corresponding to the same state in $^{10}$N with the $^{14}$B ejectile in its excited state, only makes the quality of the fit worse.

However, the spectrum can also be fitted considering only the contribution of the three- and four-body fragmentation decay, without including any peak. This calculation is presented in Fig. 5(b). The quality of the fit is worse mainly in the peak region and the total $\chi^2$ between $E_{decay}=0$ and 6.3 MeV is 18 for ten degrees of freedom. The best fit occurs for an excitation energy of 0.33 MeV for the decay products, which does not correspond to any possible excited state. If we impose the decay products to be in ground state, the total $\chi^2$ will be 19 for ten degrees of freedom.

From the point of view of probability or likelihood ratios, only the difference between the total $\chi^2$ values matters. The difference in total $\chi^2$ values (with the same number of degrees of freedom) is $\Delta\chi^2=8.2$ between the best fit with and that without resonance. This difference $\Delta\chi^2$ can be related to the likelihood ratio $k$ [18],

$$k=\exp(\Delta\chi^2/2)=60. \tag{12}$$

The likelihood ratio $k=60$ corresponds to an evidence strong enough to cause a $k$-fold increase in a prior probability ratio. Thus the likelihood ratio of 60 means that it is 60 times more probable that there is a resonance in the experimental spectrum than the contrary, if there is no prior bias on the probability ratio. Thus the probability of occurrence of the resonance is 98.4% against 1.6% for the absence of the resonance, for a total 100% of probability.

The broad resonance with $\Gamma_l(E_r)=2.3$ MeV is compatible with the supposed shell structure of $^{10}N_{g.s.}$, where the last proton is expected to be in the intruder $2s_{1/2}$ orbital located below the $1p_{1/2}$ and $1d_{5/2}$ orbitals. The ''dimensionless reduced width'' $\theta^2$, defined by [19] as $\theta_0^2=(\hbar^2/\mu a^2)^{-1}\gamma_0^2$, where $\mu$ is the reduced mass and $a$ is the matching radius of 4.46 fm, has a value of 0.5(3) for the $\gamma_0^2=1.2$ MeV. The single particle value of $\theta^2$ should be about 1 for an $s$ state, while for a $p$ state a smaller value would be expected. The same quality of fit could also be obtained by an $l=1$ resonance at the same position and with $\gamma_1^2=4(3)$ MeV. The penetrability factor decreases by about a factor of 2 between an $l=0$ and $l=1$ proton at this energy. The ''dimensionless reduced width'' $\theta_1^2=(\hbar^2/\mu a^2)^{-1}\gamma_1^2=1.7(13)$. Thus considerations on the width of the resonance cannot decide between $l=0$ or $l=1$, both are possible within the precision. The shell model calculations [20,21] predict the lowering of the $2s_{1/2}$ level below the $1p_{1/2}$, producing a $J^\pi=2^-$ ground-state for $^{10}$N.

## IV. CONCLUSION

We conclude that evidence of the $^{10}$N ground state resonance is found in the energy spectrum of the $^{14}$B ejectiles resulting from the $^{10}$B($^{14}$N,$^{14}$B)$^{10}$N reaction. The amount of contamination of the $^{10}$B target with $^{11}$B and $^{16}$O was precisely determined by the ($^{14}$N,$^{12}$B) and ($^{14}$N,$^{13}$B) reactions on the $^{10}$B, $^{11}$B, and $Li_2O$ targets. The $^{14}$B spectra on $^{11}$B and $Li_2O$ targets were normalized and subtracted from the spectrum measured on the $^{10}$B target.

The peak observed in the subtracted spectrum has statistical significance of $4.0\sigma$. The likelihood ratio of 60 is calculated from the difference between total $\chi^2$ values ($\Delta\chi^2=8.2$) of the the best fit with or without resonance. This means it is 60 times more probable to have a peak in the spectrum, than not to have it.

The peak is a broad structure and was fitted by an $l=0$ resonance at $E_r=2.6(4)$ MeV. This resonance energy corresponds to a mass excess value of 38.8(4) MeV for the $^{10}N_{g.s.}$, very close to the Audi-Wapstra estimation, which is about 38.5(4) MeV [13]. The observed width of the resonance [$\Gamma_l(E_r)=2.3(16)$ MeV] is compatible with an $l=0$ resonance, since it yields $\gamma_0^2=1.2(7)$ MeV and $\theta_0^2=0.5(3)$.

These values are compatible with the supposed shell structure of $^{10}N_{g.s.}$, where the last proton is expected to be in the $2s_{1/2}$ orbital located below the $1p_{1/2}$ and $1d_{5/2}$ orbitals. The cross section of the $^{10}$N ground-state production through the $^{10}B(^{14}N,^{14}B)^{10}N$ reaction is $0.7 \pm 0.2$ nb/sr.

**ACKNOWLEDGMENTS**

We thank H. G. Bohlen for many discussions. J.M.O., G.F.L., and V.G. thank FAPESP, and A.M.L. and A.N.O. thank EPSRC.

[1] A. Lépine-Szily, J. M. Oliveira, Jr., A. N. Ostrowski, H. G. Bohlen, R. Lichtenthäler, A. Blazevic, C. Borcea, V. Guimarães, R. Kalpakchieva, V. Lapoux, M. MacCormick, F. de Oliveira Santos, W. von Oertzen, N. A. Orr, P. Roussel-Chomaz, Th. Stolla, and J. S. Winfield, Phys. Rev. Lett. **80**, 1601 (1998).

[2] J. M. Oliveira, Jr., A. Lépine-Szily, H. G. Bohlen, A. N. Ostrowski, R. Lichtenthäler, A. Di Pietro, A. M. Laird, G. F. Lima, L. Maunoury, F. de Oliveira Santos, P. Roussel-Chomaz, H. Savajols, W. Trinder, A. C. C. Villari, and A. de Vismes, Phys. Rev. Lett. **84**, 4056 (2000).

[3] K. H. Wilcox, R. B. Weisenmiller, G. J. Wozniak, N. A. Jelley, D. Ashery, and J. Cerny, Phys. Lett. **59B**, 142 (1975).

[4] F. C. Barker and G. T. Hickey, J. Phys. G **3**, L23 (1977).

[5] A. I. Amelin, M. G. Gornov, Yu. B. Gurov, A. L. Ilin, P. V. Morokhov, V. A. Pechkurov, V. I. Savelév, F. M. Sergeev, S. A. Smirnov, B. A. Chernyshev, R. R. Shafigullin, and A. V. Shishkov, Sov. J. Nucl. Phys. **52**, 501 (1990).

[6] B. M. Young, W. Benenson, J. H. Kelley, N. A. Orr, R. Pfaff, B. M. Sherrill, M. Steiner, M. Thoenessen, J. S. Winfield, J. A. Winger, S. J. Yennello, and A. Zeller, Phys. Rev. C **49**, 279 (1994).

[7] H. G. Bohlen, A. Blazevic, B. Gebauer, W. von Oertzen, S. Thummerer, R. Kalpakchieva, S. M. Grimes, and T. N. Massey, Prog. Part. Nucl. Phys. **42**, 17 (1999).

[8] H. G. Bohlen, W. von Oertzen, Th. Stolla, R. Kapakchieva, B. Gebauer, M. Wilpert, Th. Wilpert, A. N. Ostrowski, S. M. Grimes, and T. N. Massey, Nucl. Phys. **A616**, 254c (1997).

[9] R. A. Kryger, A. Azhari, A. Galonsky, J. H. Kelley, R. Pfaff, E. Ramakrishnan, D. Sackett, B. M. Sherrill, M. Thoenessen, J. A. Winger, and S. Yokoyama, Phys. Rev. C **47**, R2439 (1993).

[10] M. Thoennessen, S. Yokoyama, A. Azhari, T. Baumann, J. A. Brown, A. Galonsky, P. G. Hansen, J. H. Kelley, R. A. Kryger, E. Ramakrishnan, and P. Thirolf, Phys. Rev. C **59**, 111 (1999).

[11] M. Zinser, F. Humbert, T. Nilsson, W. Schwab, Th. Blaich, M. J. G. Borge, L. V. Chulkov, H. Eickhoff, Th. W. Elze, H. Emling, B. Franzke, H. Freisleben, H. Geissel, K. Grimm, D. Guillemaud-Mueller, P. G. Hansen, R. Holzmann, H. Irnich, B. Jonson, J. G. Keller, O. Klepper, H. Klingler, J. V. Kratz, R. Kulessa, D. Lambrecht, Y. Iefels, A. Magel, M. Mohar, A. C. Mueller, G. Münzenberg, F. Nickel, G. Nyman, A. Richter, K. Riisager, C. Scheidenberger, G. Schrieder, B. M. Sherrill, H. Simon, K. Stelzer, J. Stroth, O. Tengblad, W. Trautmann, E. Wajda, and E. Zude, Phys. Rev. Lett. **75**, 1719 (1995).

[12] J. A. Caggiano, D. Bazin, W. Benenson, B. Davids, B. M. Sherrill, M. Steiner, J. Yurkon, A. F. Zeller, and B. Blank, Phys. Rev. C **60**, 064322 (1999).

[13] G. Audi and A. H. Wapstra (private communication).

[14] N. Anyas-Weiss, J. C. Cornell, P. S. Fisher, P. N. Hudson, A. Menchaca-Rocha, D. J. Millener, A. D. Panagiotou, D. K. Scott, D. Strottman, D. M. Brink, B. Buck, P. J. Ellis, and T. Engeland, Phys. Rep. **12**, 201 (1974).

[15] L. Bianchi, B. Fernandez, J. Gastebois, A. Gillibert, W. Mittig, and J. Barrette, Nucl. Instrum. Methods Phys. Res. A **276**, 509 (1989).

[16] G. Audi and A. H. Wapstra, Nucl. Phys. **A595**, 409 (1995).

[17] Th. Delbar, Gh. Grégoire, P. Belery, and G. Paic, Phys. Rev. C **27**, 1876 (1983).

[18] R. Royall, *Statistical Evidence* (Chapman and Hill, London, 1997).

[19] A. M. Lane and R. G. Thomas, Rev. Mod. Phys. **30**, 257 (1958).

[20] B. A. Brown, in *Proceedings of the International Conference on Exotic Nuclei and Atomic Masses, Arles, France, 1995*, edited by M. de Saint Simon and O. Sorlin (Editions Frontières, Dreux, 1995), p. 451.

[21] N. A. F. M. Poppelier, A. A. Wolters, and P. W. M. Glaudemans, Z. Phys. A **346**, 11 (1993).